The *IMAGE* Mission (NASA) : design, test and results from the Far UV Spectrographic Imaging

Serge HABRAKEN[1], Etienne RENOTTE[1], Pierre ROCHUS[1], Jean-Marc DEFISE[1], Claude JAMAR[1], Jean-Claude GERARD[2], Benoît HUBERT[2], Matthieu MEURANT[2] and Serge MUNHOVEN[2]

[1]**Centre Spatial de Liège**
Université de Liège - B28
Avenue du Pré Aily
B-4031 Angleur
shabraken@ulg.ac.be

[2]**Laboratoire de Physique Atmosphérique et Planétaire**
Université de Liège - IAGL
Avenue de Cointe, 5
B-4000 Liège

KEYWORDS: polar auroras, UV imaging, instrumentation

1. ABSTRACT

This paper presents the participation of CSL (Centre Spatial de Liège) and LPAP (Laboratoire de Physique Atmosphérique et Planétaire) in the IMAGE mission. This NASA mission was successfully launched on March 25, 2000. The technological implication of CSL during the mission preparation, the scientific involvement of LPAP, especially since launch time, and early scientific results are briefly summarized.

2. INTRODUCTION

The IMAGE (**I**mager for **M**agnetopause to **A**urora **G**lobal **E**xploration) NASA mission is dedicated to the observation and understanding of the interaction between the magnetosphere and the charged particles (mainly originating from the sun's activity). One of the most spectacular visualization is the aurora formation. The CSL activities were related to the design, development, and testing of the Spectrograph Imager (SI) which is one of the far UV instruments on the spacecraft deckplate. The LPAP participation concerns the Far UV scientific instrument specifications, modeling and in-flight data analysis. In this paper, the IMAGE mission is briefly described and the SI development phases are summarized. The modeling tools and first in-flight results are described and analyzed.

3. THE IMAGE MISSION

The IMAGE spacecraft is the first medium explorer (MIDEX) from NASA. It follows the recent policy of "Better, faster, and cheaper". The definition phase started in 1996 and the satellite was launched from Vandenberg AFB on March 25, 2000.
IMAGE is the first satellite mission dedicated to imaging the Earth's magnetosphere, the region of space controlled by the Earth's magnetic field and containing extremely tenuous plasmas of both solar and terrestrial origin. Invisible to standard astronomical observing techniques, these populations of ions and electrons have traditionally been studied by means of localized measurements with charged particle detectors, magnetometers, and electric field instruments. Instead of such in-situ measurements, IMAGE employs a variety of imaging techniques to "see the invisible" and to produce the first comprehensive global images of the plasma populations in the inner magnetosphere. With these images, space scientists are able to observe, in a way never possible before, the large-scale dynamics of the magnetosphere and the interactions among its constituent plasma populations.

The IMAGE mission is intended to address three broad science questions that lie at the heart of current efforts to understand the geospace environment and its response to the solar wind:

1. What are the dominant mechanisms for injecting plasma into the magnetosphere on the time scales of substorms and geomagnetic storms ?
2. What is the directly driven response of the magnetosphere to changes in the solar wind ?
3. How and where are magnetospheric plasmas energized, transported, and lost during geomagnetic storms and magnetospheric substorms ?

To address these questions, IMAGE employs energetic neutral atom (ENA) imaging, conventional photon imaging at ultraviolet wavelengths, and radio sounding to obtain global images of the principal plasma regions and boundaries of Earth's inner magnetosphere. Changes in the latitude and local time of orbit apogee will allow the spacecraft to view the inner magnetosphere from a variety of perspectives and to focus on particular regions, processes, and phenomena.
IMAGE is flying in an elliptical polar orbit with an apogee altitude of 7.2 Earth radii (45,922 km). The location of the apogee will change during the course of the two-year mission, both in latitude and, because of the Earth's revolution about the Sun, in local time (see figure 1).

The S/C platform is composed of several instruments as depicted in figure 2.

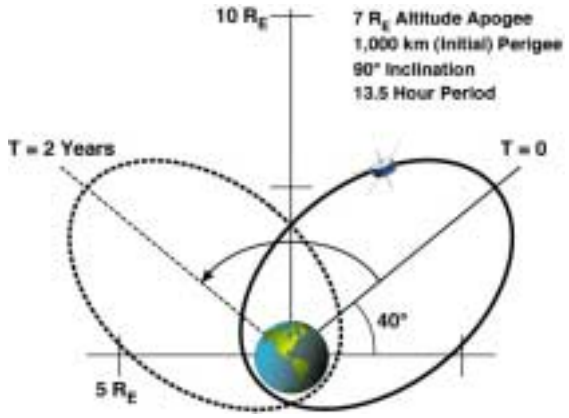

Figure 1 : Sketch of the orbit of the IMAGE spacecraft during the two-year mission.

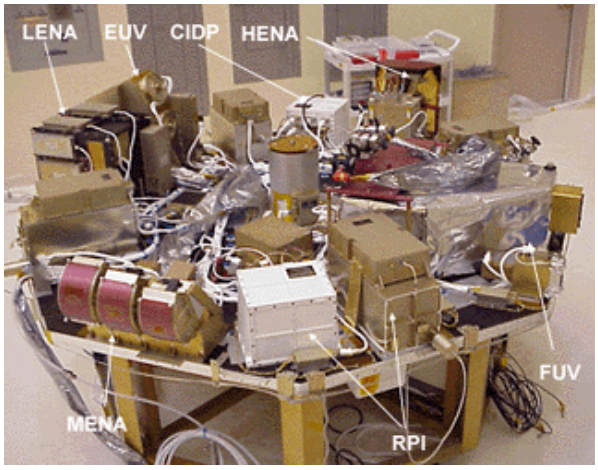

Figure 2 : The payload and the deckplate during the integration

4. FAR UV INSTRUMENTATION

Only the Far UV instruments are discussed in this paper. Narrow-band imaging of far-ultraviolet auroral emissions excited by precipitating protons and electrons at 121.8 nm and 135.6 nm, respectively (Spectrographic Imager, SI); wide-band imaging of auroral band emissions from molecular nitrogen (Wide-field Imaging Camera, WIC); measurement of geocoronal Lyman alpha emissions (GEO).
The Wideband Imaging Camera (WIC) is designed to image the whole Earth and the auroral oval. It selects the spectral range between 140 nm and 160 nm in the ultraviolet part of the optical spectrum. A

curved image intensifier is optically coupled to a CCD and the optics provides a field of view of 17x17 degrees with a spatial resolution of less than 100 km at apogee distances.
The Spectrographic Imager uses a reverse Wadsworth design [ref 1] to select the Doppler shifted HI Lyman -α line at 121.82 nm, in the ultraviolet part of the optical spectrum and to reject the non-Doppler shifted Lyman H-α from the geocorona at 121.567 nm. The field of view and resolution are similar.
The Geocorona photometers are designed to measure the atomic hydrogen Lyman-α emission of the neutral atmosphere into three different directions perpendicular to the spin axis of the satellite.

The FUV instrument and the other instruments are observing in harmony to give a global survey of the physical phenomenon related to the interaction of plasmas with the magnetosphere. Until now, the mission is a complete success with no failure and optimum performances.

5. DESIGN, FABRICATION, AND TESTS OF THE SPECTROGRAPHIC IMAGER

Design specifications :

Science requirements driving the FUV SI design were :
(1) to image the entire aurora oval from a spinning spacecraft at 7 earth radii apogee altitude;
(2) to spectrally separate the statistical noise of the intense cold geocorona (Lyman-α emissions at 121.6 nm) from the hot proton precipitation (Doppler-shifted HI Lyman-α emissions), and the NI 120 nm emission;
(3) to spectrally separate the electron (130.4 and 135.6 nm) and proton (121.6 nm) auroras.
First requirement involves a large field of view (FoV) : 15 " x 15 ".
The second requirement needs a high spectral resolution, better than 0.2 nm. The Doppler shifted Lyman-α signal to be detected is about 100 times less intense than the Lyman-α geocoronal emissions at 121.6 nm. Nitrogen emissions near 120 nm (triplet lines at 119.955, 120.022, and 120.071 nm) also have to be filtered out.
The third requirement means that the 135.6 nm signal must be isolated from the 130.4 nm signal.
The spatial resolution requirement specifies that, from 7 earth radii, the aurora oval must be imaged with a 90 km x 90 km resolution. The related angular resolution is about 7 arcmin x 7 arcmin i.e. 128 x 128 pixels.

The understanding of those scientific and technical specifications is enhanced with the description of figures 3 and 4. Figure 3 shows the WIC wide passband and the SI13 narrow band transmissions, together with a model auroral FUV spectrum. Figure 4 depicts the spectral filtering performance of the FUV SI12 based on ray-tracing simulation. These figures show how the instrument isolates the Doppler shifted Lyman-α component on the first imaging channel (figure 4) and how it is filtering the oxygen emission at 135.6 nm on the second channel (figure 3).

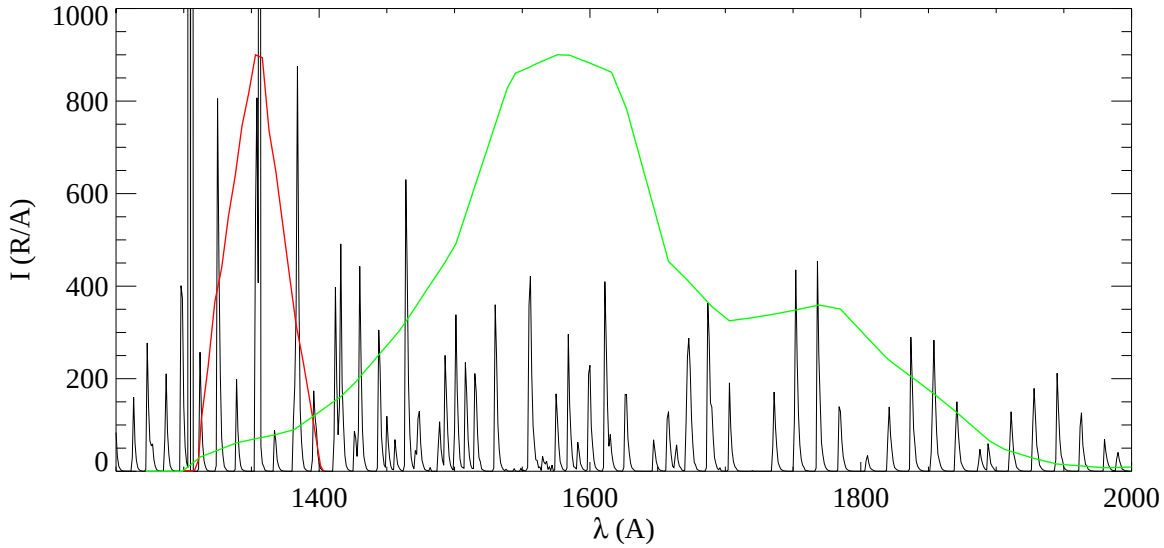

Figure 3 : FUV synthetic auroral spectrum and transmission of the wide-band WIC (green) and SI13 (red) channels. The WIC passband was selected to optimize the sensitivity and includes N_2 LBH and NI lines. The SI13 camera mainly isolates the 135.6 nm OI line.

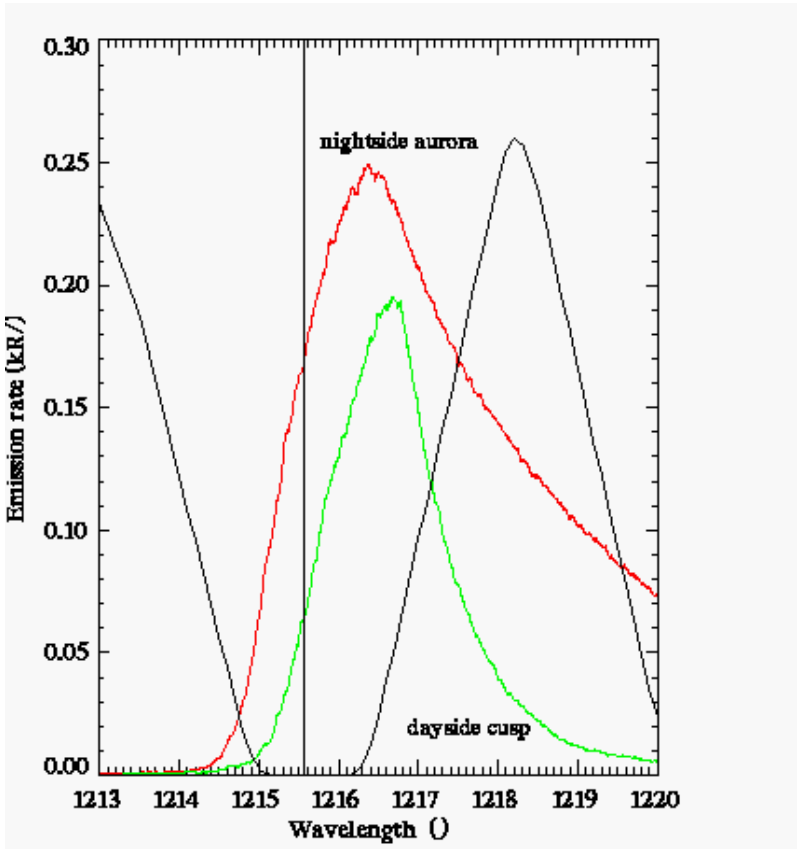

Figure 4 : FUV SI12 filtering performances (black solid line). Simulated Ly-α line profiles for a daytime cusp (green) and for a nightside aurora (red) are shown for comparison. The vertical solid line indicates the wavelength of the unshifted line profile.

Brief description of the SI optical system

Figure 5 shows a ray-tracing at 121.8 and 135.6 nm including the zero and +1 diffraction orders only (for clarity). The instrument consists of two main optical subsystems : a monochromator, and a "twin" back-imager (one at 121.8 nm and the other one at 135.6 nm).
The monochromator was designed to produce the largest dispersion, in order to reach the required high spectral resolution. Focal length is 500 mm and the grating ruling is 3600 lp/mm (holographic recording). The grating curvature is spherical; the collimator curvature is hyperbolic. The linear spectral dispersion is about 1820 µm/nm in the exit slit plane. As depicted in figure 1, a first image of the earth is produced approximately at the grating plane. The aim of the back-imager is to relay this image after diffraction by the grating, in order to obtain two spectrally separated images. Each sub-assembly of the back-imager is a two-mirror optical system. The first mirror is spherical. The second one is conical (elliptical) and off-axis. A flat folding mirror is added to the 135.6 nm imager in order to allow fitting the two detectors in close proximity. Detectors are Crossed-delay-line MCPs.
The slit configuration is made of a grill with 9 parallel slits, designed to stop the 120 and 121.6 nm (121.567 nm) lines, simultaneously. The slit spacing (period) is determined for this purpose : 0.5223 nm i.e. one third of the wavelength difference between the two lines.

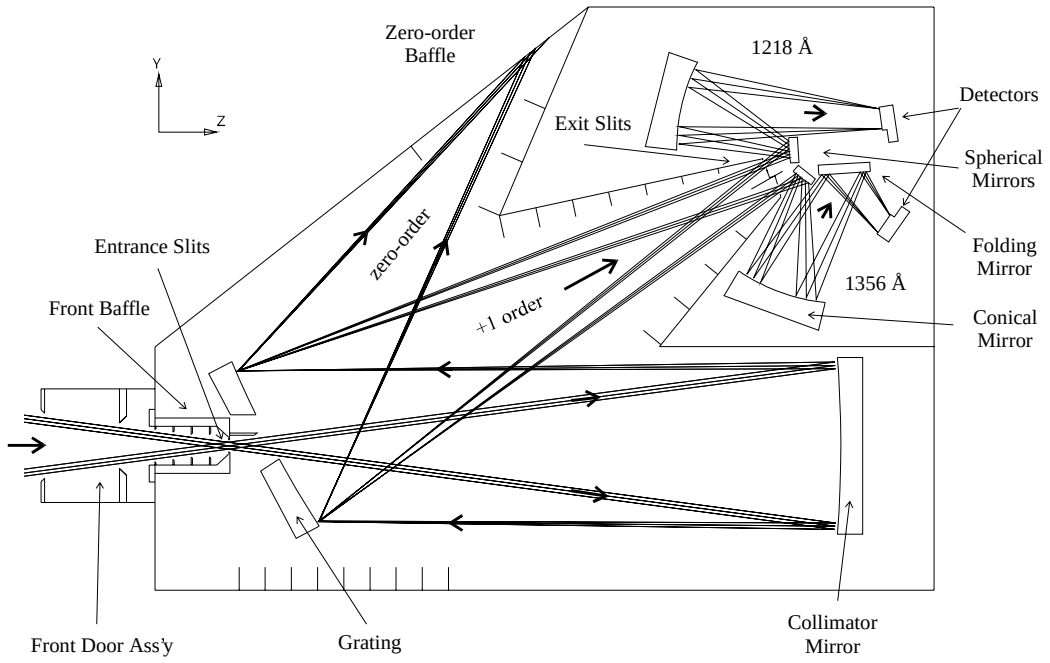

Figure 5 : Ray-tracing at 121.8 and 135.6 nm including the zero and +1 diffraction orders.

Sub-system fabrication and integration

The instrument was built thanks to the Belgian industry support. The main sub-systems were built by DSS-OIP and AMOS during year 1997. The schedule was very challenging, especially with regards to the complexity of the optical system and components. The integration and alignment were performed at the CSL facilities [ref 2].

Environmental tests [ref 3]

CSL was responsible for testing and verification of performances with respect to the baseline specifications. Due to the wavelength domain, any optical test was realised under vacuum chamber. This is especially time (and money) consuming during the alignment phase.
The instruments should be able to withstand the environmental tests without degradation of the optical characteristics. Test sequence is similar to any optical payload :

1. Vibration tests (sine and random)
2. Thermal tests (cycling, survival temperature, and operating range with optical check).

The SI successfully met the objectives, proving the very efficient work and interactions between the sub-contractors and CSL.
Figure 6 shows the instruments during vibration test preparation. A cover is, of course, to be applied on the top of it.

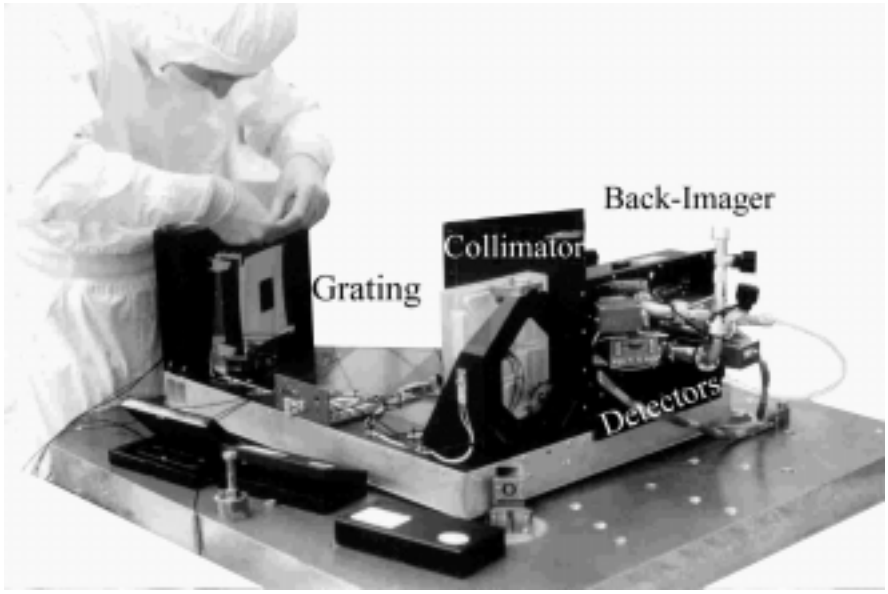

Figure 6 : Picture of the FUV-SI during shaker test preparation.

Optical calibration [ref 4]

1. Field of view/pointing :

IMAGE is a spinning spacecraft. For this reason, several instruments need to use a TDI mode (Time-Delay Integration).
In order to work properly, the TDI device needs:
- a look-up table adjusted with respect to the image distortion,
- a good knowledge of the S/C spinning axis with respect to the image.

The first requirement is performed by measuring the distortion matrix of the instrument and calculating a polynomial fitting. The second requirement is reached by measuring the FoV with respect to the reference optical cube mounted on the instrument. The resulting angular resolution of the image is about 5 arcmin x 5 arcmin. The RMS distortion fitting error is about 1.4 arcmin.
The pointing knowledge with respect to the optical cube is better than 30 arcsec.

2. Throughput response versus wavelength

The aim of this test consists in the measurement of the response of the spectrograph versus wavelength.
A throughput prediction was already established according to loss factors :

- Mirror reflectivity : about 70 % (4 reflections at 121.8 nm and 5 reflections at the 135.6 nm channel)
- Grating diffraction efficiency : about 60 %
- Theoretical transmission through the exit slits : about 90 % at 121.83 nm and 100 % at 135.6 nm.
- Detector window (MgF_2) transmission : about 50% at 121.8 nm and 70% at 135.6 nm.

The overall resulting transmission is only 7% at 121.83 nm and 135.6 nm. The last loss factor is related to the detector efficiency.

Using calibrated photo-multiplier tube (PMT), the sensitivity of the instrument was established for both channels. The count rate (count/s) of the detectors when the instrument is exposed to photon flux (photon/s/cm^2) was measured using a scanning spectrometer to isolate radiation in the wavelength range 117-140 nm. We verified that the instrument is efficiently rejecting the undesirable spectral bands. The HI Lyman-α emission is rejected to better than 98-99%. The O emission at 130.2-130.4 nm and the LBH bands at λ >140 nm are rejected to 99.9%. The NI triplet emission at 120 nm is rejected to 90-95%.

6. MODELING

A modeling effort was initiated in 1998 to provide support in the analysis and physical interpretation of the observations made with the FUV cameras. They were mostly directed at the understanding and simulation of the characteristics of the FUV emissions in the aurora.

FUV excitation in the proton aurora

The calculation of auroral electron energy degradation and excitation by solar-induced processes is based on the GLOW model [Solomon et al., 1988, Solomon, 2000] with updated cross sections. An initial energy distribution of the primary electrons is prescribed in an analytical form. The two-stream transport algorithm is based on the Banks et al.'s code, extended to higher energies for auroral calculations. The local electron flux is calculated using the two-stream approximation, solving for the upward and downward hemispherical fluxes along a magnetic field line assumed to be vertical as a function of energy. Elastic collisions, discrete energy losses from inelastic collisions and heating of the thermal electrons are considered. The energy bins and the altitude steps are variable in size. The inelastic cross sections are used in an analytical form. Many of the excitation cross sections were re-fit to reflect subsequent revisions.
The proton energy transfert code used for this study was described in details by Gérard et al. [2000]. It is based on the direct Monte Carlo method which is a stochastic implementation of the solution of the Boltzmann equations for the H^+ - H beam. Once the protons reach the thermosphere, charge exchange collisions with ambient O, O_2 and N_2 generate a population of fast H atoms which, in turn, may be converted back to energetic protons (electron stripping). The Monte Carlo proton code includes a detailed calculation of all elastic and inelastic processes for both species. A detailed treatment of the momentum transfer in all collisions makes it possible to follow the pitch angle distribution of the simulated particles. Three sources of velocity vector redistribution of the energetic protons are considered : (1) magnetic mirroring in the geomagnetic field (2) geometric spreading caused by the convergent magnetic field lines and (3) collisional angular redistribution. Doubly differential collision cross sections are used to describe proton and H atoms collisions from 0.5 to 5

keV, with extrapolations at higher energies. Ionization of the major constituents by collisions with energetic H^+ and H particles generate secondary electrons.
To simulate a combined electron-proton aurora, this population of proton-generated secondary electrons is added to the electron-generated component. Their energy loss is calculated similarly to the energetic electron component. The temperature profile and the O, O_2 and N_2 densities are calculated from the MSIS-90 model atmosphere. Ionosphere electron temperature and density are taken from the International Reference Atmosphere-1990 (IRI-90) model.

The input energy flux and characteristic mean energy of both types of charged particles for prescribed geophysical conditions and geographic location are provided by the statistical precipitation model described by Hardy et al. The resulting volume excitation rates for Ly-α, NI 149.3 nm, OI 130.4 and 135.6 nm and N_2 LBH bands are calculated including all photo- and collisional excitation processes. Finally, the emerging intensities for a given view angle are calculated taking absorption into account.

This model was applied to the midnight aurora, the noon cusp and a proton-dominated aurora for moderately disturbed conditions. We showed that in the first two cases, direct electron impact dominates the vertically integrated emission rate over the proton component, although proton excitation plays an important role at some altitudes in the daytime cusp. In afternoon regions of the auroral zone near the auroral boundary, secondary electrons due to proton ionization are the main source of FUV emissions. The energy dependence of the efficiency of LBH band emission viewed from high altitude is calculated for electron and proton precipitations. Maps of the N_2 LBH emission excited by both components are obtained and regions of proton-dominated auroral emission are identified. It was found that the distribution of the ratio of proton-induced to electron-induced brightness resembles maps of the ratio of the respective precipitated energy fluxes. Proton-dominated FUV emissions are thus located in a C-shaped sector extending from pre-noon to midnight magnetic local times with a maximum proton contribution near the equatorward boundary of the statistical electron oval. The distribution of the Ly-α/LBH ratio was found to mimic the ratio of the proton flux/total energy flux, although it is insufficient by itself to accurately determine the relative fraction of auroral energy carried by the protons.

Lyman-α brightness and lime profile modeling in the proton aurora

A stochastic direct simulation Monte Carlo method was used to solve the system of kinetic equations describing the Boltzmann equation and investigate the energy degradation of the H^+ - H beam and the formation of energetic hydrogen atoms due to auroral proton precipitation in the aurora. A key component of this model is the stochastic treatment of the scattering angle in momentum and charge transfer collisions. The Ly-α line profile is to a large extent controlled by the angular properties of the scattering process. The extent of the blue wing is considerably more important in the more realistic stochastic approach. The emerging synthetic Lyman-α line profile is calculated by numerical integration of the obtained source functions along the line of sight. The backscattered atoms (blue shift) are produced by (1) collisions of protons which have reached their mirror point and travel up the magnetic field line, (2) particles which have suffered successive scattering collisions and whose pitch angle has finally exceeded 90° and (3) a small component of particles which travelled across magnetic field lines and progressively increased their pitch angle above 90°.

The Ly-α line profile calculated for two cases based on the statistical proton energy distribution given by Hardy et al. at two different geomagnetic local times is shown in figure 4. The midnight proton aurora is characterised by a relatively hard (E = 16.1 keV) precipitation for an energy flux of 0.7 erg cm^{-2} s^{-1}. The corresponding Ly-α profile exhibits a wide red-shifted wing extending over 10 Å from

rest wavelength. The polar cusp aurora with its softer proton distribution (E = 2.2 keV) and lower-energy flux (0.15 erg cm^{-2} s^{-1}) presents a different Ly-α signature. In this case, the total brightness is substantially less than in the nighttime aurora. The line full width at half maximum is about 1.5 Å compared with 3.9 Å for the midnight Ly-α profile.
Our results show that the Ly-α profile reflects both the energy and the pitch angle distribution of the protons interacting with the atmosphere (figure 7). Stochastically simulated collisional spreading causes the Ly-α peak to move to the rest wavelength as energy increases, due to the large number of collisions encountered by the energetic H^+ - H beam as it moves toward the dense lower-altitude atmosphere.

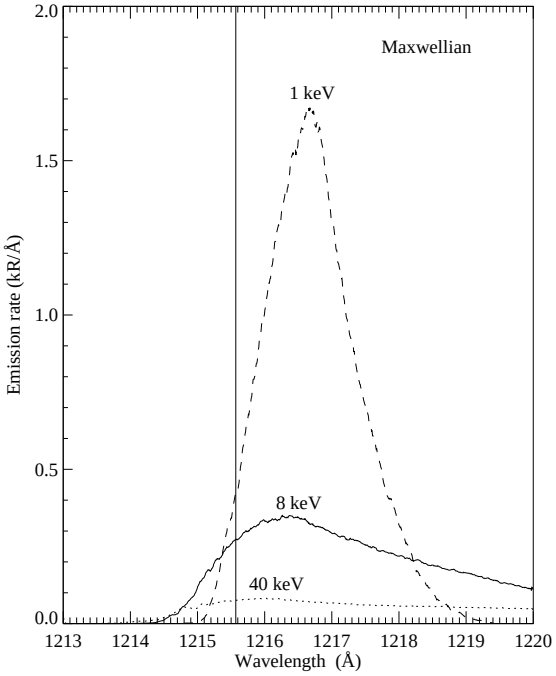

Figure 7*: Lyman-a line profile calculated with the Monte Carlo model for initial proton Maxwellian energy distributions with three different characteristic energies*

7. FLIGHT RESULTS AND PRELIMINARY ANALYSIS

The FUV instrument has been providing excellent quality observations since early May 2000. The signal is at least as high as was expected from the laboratory calibration and model simulations. During most orbits, FUV images are obtained over a period of nearly 10 hours. They consist of global views of the north pole and close-up observations near perigee. Figure 8 shows an example of an aurora observed near apogee simultaneously in the three FUV channels.

A crucial test was to compare the morphologies observed by SI12 and the other two cameras. Figure 9 illustrates a feature commonly observed in the FUV images. The narrow arc filamentary structures frequently seen in the nighttime electron aurora (WIC, SI13) have no counterpart in the proton (SI12) aurora. The proton aurora is usually characterized by a broad diffuse oval structure partly overlapping the electron precipitation regions.

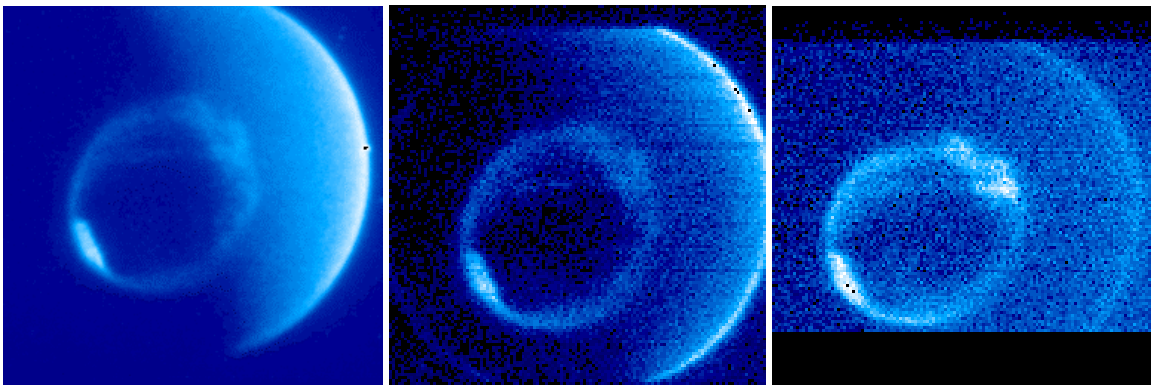

Figure 8 : Image obtained simultaneously on September 18, 2000. From left to right: WIC, SI13 and SI12. Note the similarity between the WIC and SI13 morphologies. In contrast, the bright feature observed in the early afternoon main oval in SI12 (proton aurora) is not seen in the WIC and SI13 channels.

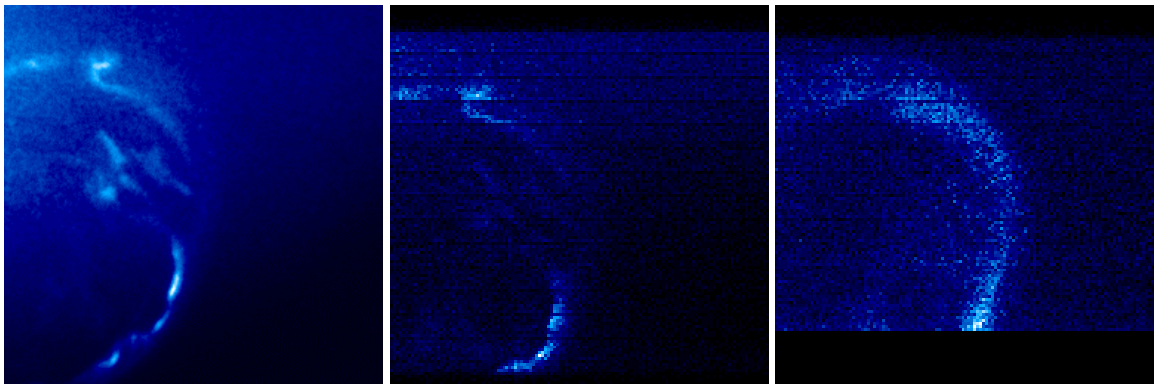

Figure 9: same as fig; 8 for June 7, 2000. The thin arc structure in WIC and SI13 (left panels) are not observed in SI12, indicating that these features (probably inverted-V structures) are excited by electrons only

So far, data analysis has concentrated on two aspects: (1) comparison with *in-situ* particle measurements from the FAST satellite and (2) observation of the proton morphology during a substorm.

Comparison with FAST data.

FAST orbit 15226 (June 24, 2000, 0610-0650 UT) is the first of two orbits analyzed for this investigation. Figure 10 shows these brightness tracks along the FAST footprint for all three FUV systems. The bright signal in the dusk pre-midnight part of the SI12 image (right part of image) is furthermore an indicator that this channel is not sensitive to electron induced aurora, because the same region is comparably dim in the WIC and SI13 images. Additionally, Figure 10 shows the downgoing electron and ion energy fluxes. The fluxes were mapped down to 100 km altitude to be comparable to the optical emissions they produce in the upper atmosphere.

There is a clear peak of ion precipitation at the equatorward boundary of the auroral oval which coincides well with the peak in the SI12 signal. Further poleward the ion precipitation decreases and overlaps with the electron precipitation which, in contrast to the ions, peaks at the poleward boundary of the oval. The energy flux at the dayside part of the oval is much smaller than on the nightside. From just a the visual comparison in the WIC channel it is clear that the two peaks in the WIC signal do not correspond to a similar structure in the electron energy flux.

The electron and ion spectra from the FAST measurements were used as inputs for the code of the production of auroral emissions in the FUV range described before [Hubert et al., 2000]. Each individual spectrum in the loss cone measured by the FAST satellite was used to calculate the emission rate of the N_2 LBH, OI, and NI line brightness excitation processes. The emerging intensities for a nadir observation are obtained by integration along the line of sight. The simulations indicate that the LBH and 135.6 nm emissions may contain significant contributions from proton excitation. Taking the expected brightness from simulations with the electron precipitation only, we obtain a good agreement at the dayside and at the poleward part of the nightside auroral oval. At the equatorward part of the nightside auroral oval however, the expected signal from electron precipitation is only about 60-70 % of the measured WIC signal. If the simulation also includes the ion precipitation, then a much better overall agreement between the expected obtained WIC signal is reached.

This comparison also shows that under certain circumstances the precipitating protons may produce significant amounts of auroral emissions usually associated with electron precipitation. For the case of IMAGE FUV the presence of the SI12 channel allows for the determination of the proton flux and a corresponding correction to the electron flux estimated from the WIC and SI13 channels.

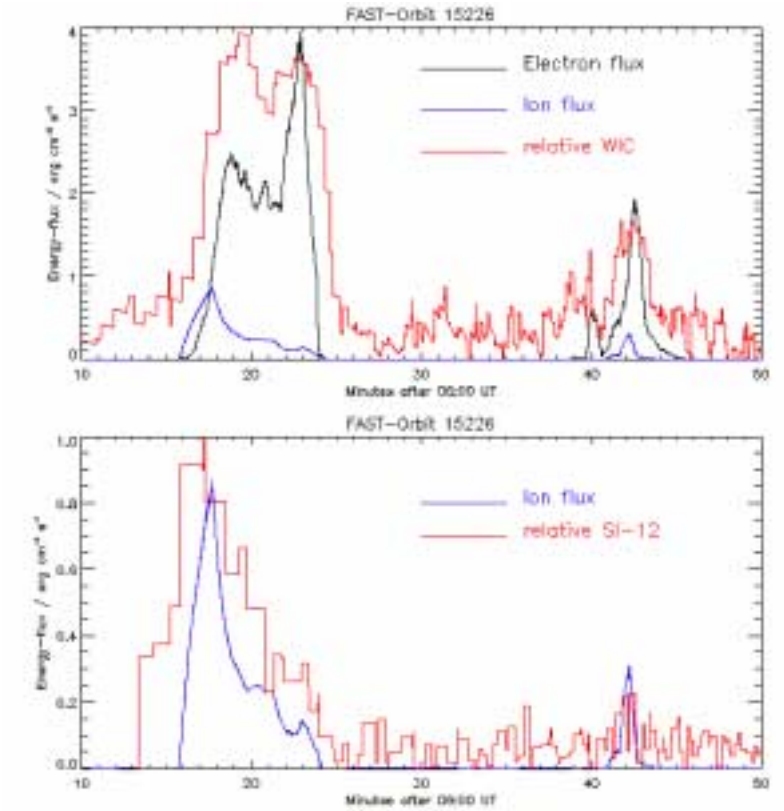

Figure 10 : *Brightness tracks along the FAST footprint during the transit through the FUV images. Also shown are the averaged measured electron and ion energy fluxes which were mapped down from the FAST location to 100 km altitude.*

Global observation of proton morphology during a substorm

On June 28, 2000 the IMAGE spacecraft was climbing towards apogee when the sequence of images shown in Figure 11 were taken. At 1956 the aurora is quiet with very little activity in the broad band LBH except the early afternoon where we see evidence of some structuring in the form of possible Kelvin Helmholtz waves or perhaps large spacing spatially periodic auroral distortions. In the first images the midnight part of the proton oval is superimposed on this enhancement. The proton oval is fairly uniform and diffuse. It is located slightly equatorward of the electrons on the dusk evening side but seems to be collocated with the electrons at midnight and in the morning. At 2000 UT we see the first sign of a breakup which started near midnight.

The first response of the proton aurora to the substorm occurs near midnight local time at 2004 UT. The very bright spot in the WIC does not have a counterpart in the SI12 image. At 2015 the SI12 aurora touches the 75° latitude circle while the electron aurora is still at 72-73°. The image pair for 2023 UT shows that there is a faint region of proton precipitation which is at the same or higher latitude as the bright electron surge. However, the bulk of the proton intensification takes place at the original location of the proton aurora. It is interesting to note that the intensity of the proton aurora at this time is brighter duskward, consistent with the idea that freshly injected protons would drift. duskward. At 2031 the poleward surging WIC aurora is brightest at the poleward edge of the surge while the SI aurora is brightest equatorward and duskward.

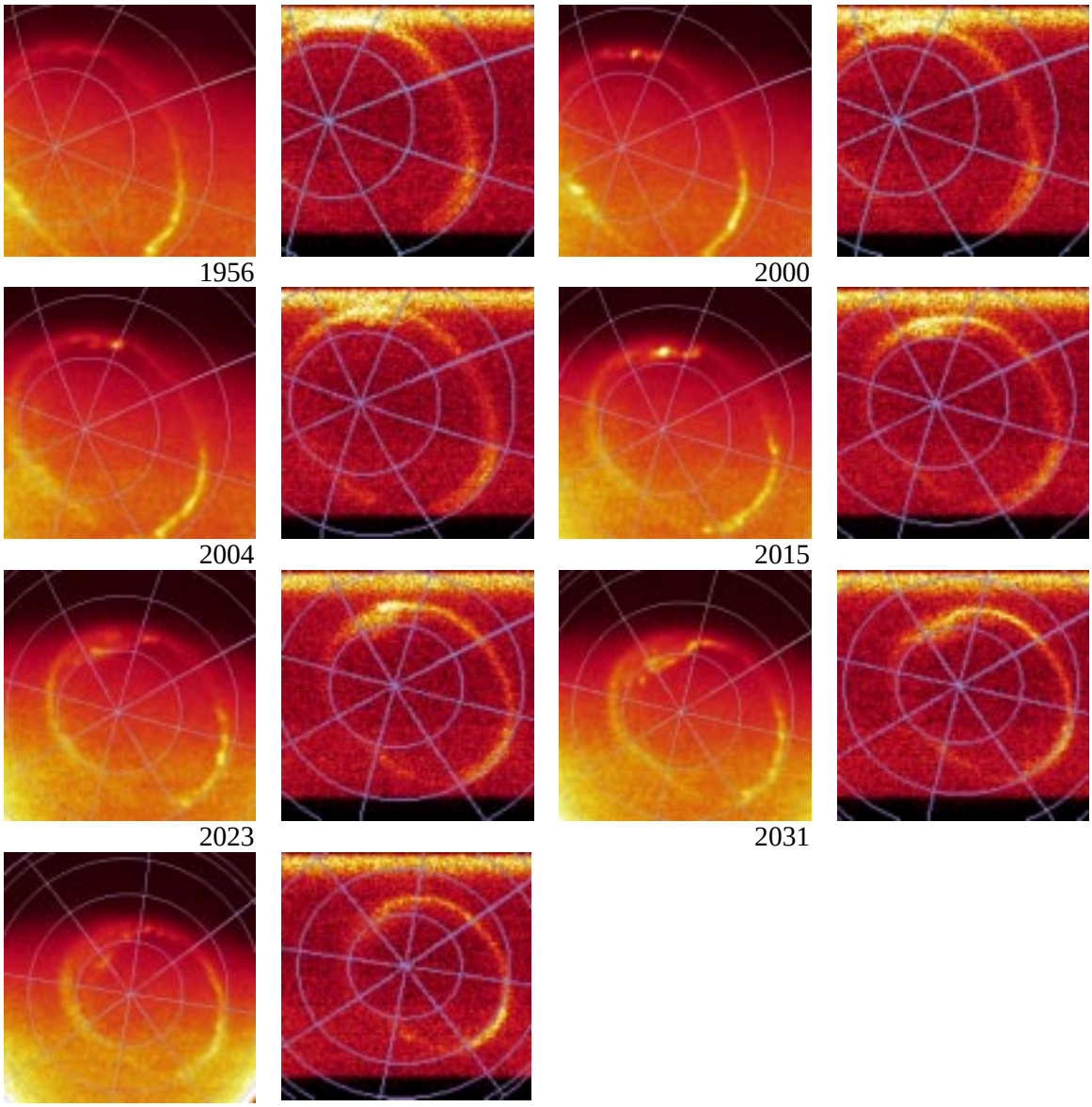

Figure 11*: Collage of selected image pairs from the period including a substorm which occurred* on June 28, 2000. *On the left of the figure are shown the WIC images, and on the right the SI12 images of the proton aurora. In these presentations the noon-midnight is very closely aligned with the vertical of the page (midnight is approximately at the top). The bright zone at the top of the SI frames is due to geocoronal Ly-*α *leak.*

At 2047 the electron aurora reaches its highest latitude and the proton aurora is distinctly left behind. A very interesting and perhaps unrelated event is shown by the image pair from 2049 when a sudden brightening occurs in the dusk sector. This brightening is very intense in the WIC image and it has a fainter counterpart in the SI12 channel

In agreement with prior work, these data show that the proton aurora is generally equatorward of or collocated with the quiescent electron precipitation. In the afternoon evening hours the proton precipitation was equatorwards of the quiescent aurora produced by the electrons. The azimuthal

extent of the proton and electron aurora is also interesting. The first image, which shows the entire auroral oval, was taken at 2015. A bright region in both protons and electrons is present in the early afternoon; this is the location of the afternoon arc. On the night side the protons fill the evening half of the oval and the electrons mainly fill the morning side. This is in agreement with the azimuthal drift of electrons and protons injected at midnight.

The initial brightening of the substorm at 2004 UT was embedded in the proton precipitation. Particle measurements show that these protons are energized by convection and they are generally well inside in the magnetosphere in the region of geosynchronous altitude satellites. The fact that the substorm initiation occurs in or near the zone of precipitating protons seriously constrains substorm theories. Close examination of the image pairs taken at 2000 and 2004 UT shows that the proton aurora was slightly equatorward of the bright patch development at the onset of the substorm. It appears that the proton aurora expands poleward with the electron aurora surge but it appears faint and diffuse. The first sign of intensification of the proton aurora takes place at 2023 a full 20 minutes after the initiation of the electron intensification. It seems to take about 20 minutes for the protons to experience substorm acceleration.

Protons and electrons participate in the poleward expansion of the aurora but the protons slow down and the poleward edge of the surge is populated only by electrons. By 2047 UT it is clear that the proton aurora is absent in the leading edge of the expanding electron auroral. Another remarkable feature is the brightening in the afternoon side at 2049. This is a sudden auroral intensification which is not accompanied by poleward expansion and therefore qualifies as a pseudo-breakup.

In summary this is the first example of studies which are made possible by the IMAGE FUV system. It demonstrates its capability in recording electron and proton aurorae and follow their time dependent development.

8. CONCLUSIONS

The Spectral Imager in the FUV-IMAGE system was largely designed, tested and calibrated at CSL (Ulg) in the frame of the PRODEX program. Although the data analysis is still in its early phase, the first months of operations of the instrument clearly demonstrate its excellent performances. In particular, the SI12 camera makes it possible for the first time to globally image the morphology of the auroral proton precipitation. The capability opens new windows on the monitoring and understanding of the magnetospheric processes leading to the polar aurora. The preparatory program developed at LPAP provided the opportunity to develop and test models which are now being used for the analysis and physical interpretation of the IMAGE-FUV data. It is expected that a very rich harvest of observations will be generated by this mission and that significant progress in the understanding of the auroral phenomena will be made. The Belgian involvement will be very fruitful both technically and scientifically.

9. REFERENCES

[1] S. Habraken, C. Jamar, P. Rochus, S. Mende, M. Lampton, "Optical Design of the FUV Spectrographic Imager for the IMAGE Mission," *EUV,X-Ray, and Gamma-Ray instrumentation for astronomy VIII,* O.H.W. Siegmund and M.A. Gummin, ed., Proc. SPIE **3114**, 544-553 (1997).

[2] S. Habraken, Y. Houbrechts, E. Renotte, C. Jamar, S. Mende, H Frey, and O. Siegmund, "Alignment and Performances of the FUV Spectrographic Imager for the IMAGE Mission," *EUV,X-Ray, and Gamma-Ray instrumentation for astronomy IX,* O.H.W. Siegmund and M.A. Gummin, ed., SPIE **3445** (1998).

[3] E. Renotte, S. Habraken, and P. Rochus, "Design and Verification of the Far Ultraviolet Spectrographic Imager (FUV-SI) for the IMAGE Mission," *EUV,X-Ray, and Gamma-Ray instrumentation for astronomy IX,* O.H.W. Siegmund and M.A. Gummin, ed., SPIE **3445** (1998).

[4] S. Habraken, Y. Houbrechts, E. Renotte, M-L Hellin, A. Orban, P. Rochus, S. Mende, H. Frey, S. Geller, and J. Stock, "Optical Calibration of the FUV Spectrographic Imager for the IMAGE Mission," *EUV,X-Ray, and Gamma-Ray instrumentation for astronomy X,* O.H.W. Siegmund ed, SPIE **3765**-53 (1999).

10. BIBLIOGRAPHY

10.1 Peer reviewed articles

J.C. Gérard, B. Hubert, D.V. Bisikalo and V.I. Shematovich, A model of the Lyman-α line profile in the proton aurora, *J. Geophys. Res*., 105, 15,795-15,805 (2000).

B. Hubert, J.C. Gérard, D.V. Bisikalo,V.I. Shematovich, and S. C. Solomon, The role of proton precipitation in the excitation of auroral FUV emissions (2000).

S.B. Mende, H. Heetderks, H.U. Frey, M Lampton, S.P. Geller, S. Habraken, E. Renotte, C. Jamar, and P. Rochus,, J. Spann, S.A. Fuselier, J-C Gérard, G.R. Gladstone, S. Murphree, and L. Cogger, "Far Ultraviolet Imaging from the IMAGE spacecraft : 1 System Design," Space Science Reviews, **91** / 1-2, 243-270 (2000).

S.B. Mende, H. Heetderks, H.U. Frey, M Lampton, S.P. Geller, R. Abiad, O.H Siegmund, S. Habraken, E. Renotte, C. Jamar, and P. Rochus, J-C Gérard, R. Sigler, and H. Lauche, "Far Ultraviolet Imaging from the IMAGE spacecraft : 3. Spectral Imaging of Lyman-α and OI 135.6 nm," Space Science Reviews, **91** / 1-2, 287-318 (2000).

S. B. Mende, H. U. Frey, M. Lampton, J.-C. Gérard, B. Hubert, S. Fuselier, R. Gladstone, J. L. Burch, Global observations of proton and electron auroras in a substorm, Geophys. Res. Lett. (2000).

H.U. Frey, S.B. Mende, C.W. Carlson, J.-C. Gérard, B. Hubert, J. Spann., R. Gladstone, T.J. Immel, « The electron and proton aurora as seen by IMAGE-FUV and FAST », *Geophys. Res. Lett*. (2000).

10.2 Conference papers

S. Habraken, C. Jamar, P. Rochus, S. Mende, M. Lampton, "Optical Design of the FUV Spectrographic Imager for the IMAGE Mission," *EUV,X-Ray, and Gamma-Ray instrumentation for astronomy VIII,* O.H.W. Siegmund and M.A. Gummin, ed., Proc. SPIE **3114**, 544-553 (1997).

S. Habraken, Y. Houbrechts, E. Renotte, C. Jamar, S. Mende, H Frey, and O. Siegmund, "Alignment and Performances of the FUV Spectrographic Imager for the IMAGE Mission," *EUV,X-Ray, and Gamma-Ray instrumentation for astronomy IX,* O.H.W. Siegmund and M.A. Gummin, ed., SPIE **3445** (1998).

E. Renotte, S. Habraken, and P. Rochus, "Design and Verification of the Far Ultraviolet Spectrographic Imager (FUV-SI) for the IMAGE Mission," *EUV,X-Ray, and Gamma-Ray instrumentation for astronomy IX,* O.H.W. Siegmund and M.A. Gummin, ed., SPIE **3445** (1998).

S. Habraken, Y. Houbrechts, E. Renotte, M-L Hellin, A. Orban, P. Rochus, S. Mende, H. Frey, S. Geller, and J. Stock, "Optical Calibration of the FUV Spectrographic Imager for the IMAGE Mission," *EUV,X-Ray, and Gamma-Ray instrumentation for astronomy X, Paper N° 3765-53.* O.H.W. Siegmund ed., SPIE meeting, Denver, 18-23 July 1999.

RELATED WEB SITES

http://sprg.ssl.berkeley.edu/image/
http://image.gsfc.nasa.gov/
http://image.gsfc.nasa.gov/poetry/
http://pluto.space.swri.edu/IMAGE/index.html

FUNDING AND ACKNOWLEDGMENTS:
The CSL and LPAP activities in the IMAGE project were funded by the Belgian OSTC through the ESA Prodex programme.
J.C. Gérard is supported by the Belgian Fund for Scientific Research (FNRS).
V. Shematovich and D. Bisikalo played an active role in the development of the numerical codes used for the FUV data analysis.